Official journal of the JHL 2689-9620
www.light-am.com

Article Open Access

Effect of near-field optical angular momentum on molecular junctions

Jianchen Zi[1], Michaël Lobet[2], Luc Henrard[2], Zhiqiang Li[1], Chenhui Wang[1], Xiaohong Wu[3] and Hai Bi[1,*]

Abstract

The role of molecular junctions in nanoelectronics is most often associated with electronic transport; however, their precise characterisation hinders their widespread development. The interaction of light with molecular junctions is a supplementary factor for the development of molecular switches, but it has rarely been addressed. The influence of light interaction with molecular junctions on the response of molecules in the near field was demonstrated by properly characterising the optical angular momentum at the junctions. Consequently, the molecular switching dynamics were observed in the Raman signatures of the conducting molecules. The illumination geometry and voltage applied to the junction were changed to demonstrate numerically and experimentally how the Raman intensity can be turned ON and OFF with a difference of nearly five orders of magnitude. These molecular-scale operations result from the combined interaction of a current-induced electronic rearrangement in the molecular junction and a plasmonically enhanced electromagnetic field near the tip of the junction. This study of the effect of optical angular momentum on the near field of the molecular junction shows significant potential for the development of molecular electronics.

Keywords: Molecular junctions, Near-field enhancement, Raman spectroscopy, Localised angular momentum

Introduction

Understanding and controlling the molecular switching of a single molecule is fundamental for the development of molecular logic operations and for the further development of nanoscale computation. Recently, most research has focused on investigating molecular junctions based on electronic characterization[1–4]. In addition to applied voltage, light can influence the molecular state and characterises molecular states complementarily[5–8]. However, most classical optical spectroscopy methods are limited by diffraction, which makes it difficult to characterise nanoscale systems with ultrahigh spatial resolution. Near-field-enhanced techniques based on local surface plasmon (LSP) can break the diffraction limit and provide an excellent solution for ultramicroscopy[9]. Such near-field-enhanced techniques provide highly accurate methods for nano areas, such as coherent manipulation, processing, and measurement techniques for tunnelling currents in nano electronic devices[10–13].

In the past decade, many researchers have reported nanoscale optical resolution based on near-field-enhanced techniques with an apertureless probe tip[14–18]. At such a nanoscale, the light field is intensely bounded by the LSP modes around the apex of the apertureless probe tip. The near field, especially its electric field component, is dramatically enhanced and, consequently, is used for

Correspondence: Hai Bi (bihai@jihualab.com)
[1]Jihua Laboratory, No.28 Huandao South road, Nanhai district, Foshan 528200, China
[2]Department of Physics and Namur Institute of Structured Materials, University of Namur, Rue de Bruxelles 61, 5000 Namur, Belgium
Full list of author information is available at the end of the article.

efficient nondestructive detection of molecular states with local Raman spectroscopy[19–22]. Actually, the Raman signal of the molecular junction can be strongly affected by the electrode geometry and the excited plasma[23,24]. Simultaneously, asymmetric LSP modes can introduce a near-field angular momentum[25–27], which can have an effect on nearby molecules[28–30]. Recently, the Raman response of oligo(phenylene ethynylene)-3 (OPE-3) molecular junctions with near-field angular momentum coupling was reported[31]. It was observed that such the coupling has an effect on the transport electrons in molecular junctions. However, the combined effects of the applied voltage and local electromagnetic field on the switching behaviour of the molecular junction must be investigated from electrical transport and electromagnetic viewpoints. Furthermore, the impact of the polarisation of light and the symmetry properties of the near-field system remain unexplored.

In this study, the combined effect of the near-field optical angular momentum and the bias voltage on the Raman response of a single molecular junction, creating a molecular switch, was investigated. Using a homemade molecular junction spectroscopy (MJS) platform[31], optical and electrically driven conformational switching in the covalently linked metal–molecule–metal junctions of 2,2',2'',5'-tetramethyl-[1,1':4',1''-terphenyl]-4,4''-dithiol (TM-TPD) was characterised. The non-π-conjugated molecular 'wire' of TM-TPD electrically connects the gold-coated tip of a tunnelling microscope to a gold substrate (Fig. 1). Previously, a TM-TPD molecular junction was used[17] to confirm a prior observation that the Raman activity of the molecule can be turned ON and OFF using the biased voltage because of the molecular conjugation during charge transport through molecular orbitals. In this study, it was further demonstrated that the molecular switch can be manipulated using an optical input. The effects of both the polarisation of light and the subsequent symmetry properties of the electromagnetic near field were investigated and used to control the switching behaviour. This change in the Raman response of the junction is associated with a modification of the conformation of the molecule. This is further supported by density functional theory (DFT) simulations. Consequently, both the polarisability tensor and the Raman response are tuned. By changing both the illumination side and the voltage applied to the junction, the Raman intensity can be turned ON and OFF with a difference of nearly five orders of magnitude between the two states (Fig. 2a).

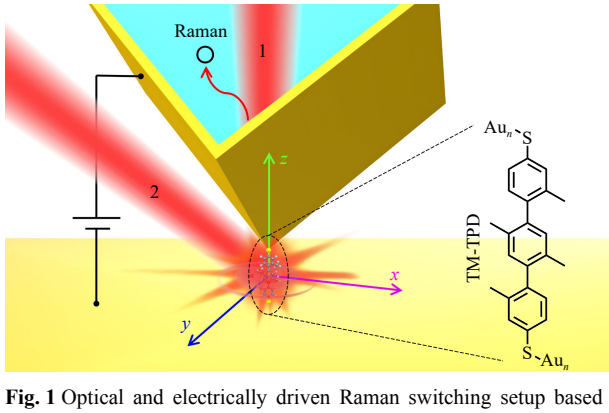

Fig. 1 Optical and electrically driven Raman switching setup based on molecular junction. The schematic diagram shows conformational switching in a tip−molecule−substrate junction with Raman readout via optical coupling of the optical angular momentum to the molecule. Laser illuminations from the top (channel 1) or the side (channel 2) with a 45° incident angle are shown accordingly. The *z*-axis is defined as perpendicular to the gold substrate, and the triangular-pyramid tip is mirror-symmetric along the *x*-axis.

Results and discussion

Molecular junction Raman spectroscopy for top or side illumination

Upon preparation of a self-assembled monolayer of thiolated TM-TPD on an amorphous gold substrate, single molecules are contacted by an apertureless, gold-coated, triangular pyramid (TP)-shaped, near-field tip. The probe tip has three roles: serving as an electrical contact, light source input, and light collector output. Contacts between the tip and single molecules occur spontaneously and are stabilised by piezoelectric control in a typical timeframe of minutes under ultrahigh vacuum conditions. Unpolarised 632.8-nm laser inputs can be sent either from the top (channel 1) or from the side (channel 2) through the probe tip (Fig. 1). A near-field-enhanced Raman spectrum is collected from the top and used as the output. As several results have shown in recent years[17,31–33], the entire system is reliable for simultaneously measuring the electrical and optical properties of molecular junctions. With this setup, one can simultaneously measure the conductance and Raman spectra of molecular junctions. Using conductance measurements and statistical methods, the conductance of a single-molecule junction of TM-TPD was identified. This method is widely used to confirm the conductivity of single molecules. During the Raman measurements, the conductance of the molecular connections is maintained at a constant value to ensure that the Raman spectra are from the same molecular junction. In addition, p-terophenyl derivatives do not tend to form intermolecular π–π stacking because of the nonplanarity formed by twisting feet between adjacent benzene rings. Thus, the switching behaviour can be identified as a single-molecule junction

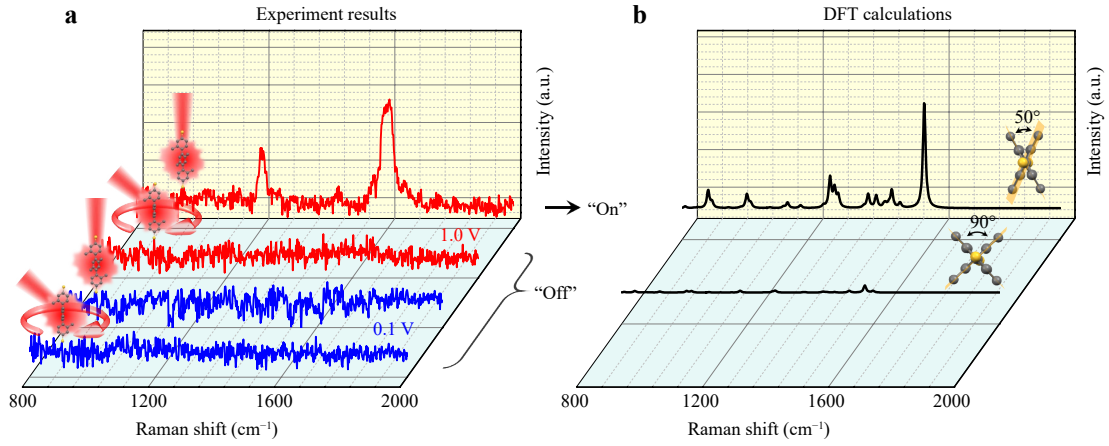

Fig. 2 Optical and electrically driven Raman switching in the molecular junction spectroscopy setup. **a** Raman spectra of TM-TPD corresponding to different voltage and illumination geometries. The red and blue lines are for voltages of 1.0 and 0.1 V, respectively, and the insets show the illumination geometries. **b** DFT calculations for the ON and OFF Raman modes. The Raman signature is mainly dominated by the molecular conformation of TM-TPD. The dihedral angle between the benzene ring at both ends and the central benzene ring is 50° for ON mode and 90° for OFF mode (see Supporting Information SI.1 for details). By changing both the illumination side and the voltage applied to the junction, the Raman intensity can be turned ON and OFF.

and not as a supramolecular packing effect.

Fig. 2a shows the Raman spectra of the TM-TPD at different applied voltages and illumination geometries. For top illumination under a biased voltage of 1.0 V (first line from the top), a clear Raman signal was observed, which corresponds to the ON mode. However, when side illumination was adopted instead of top illumination (second line from the top), the Raman signal fell below the instrumental detection limits, turning off the Raman vibrational modes (OFF mode). For cases under a biased voltage of 0.1 V, no Raman signal was observed, regardless of the top illumination (third line from the top) or side illumination (fourth line from the top). The observed voltage-driven switching can be repeatedly turned on and off, which is limited solely by the junction stability.

According to the DFT calculation results (Fig. 2b), the ON and OFF signatures of the Raman spectra correspond to different molecular geometries[17], with a dihedral angle of 50° corresponding to the charged TM-TPD, and 90° corresponding to the neutral one (see Supporting Information SI.1 for details). The Raman signature was strongly suppressed (OFF mode) with the highly sterically hindered nonplanar neutral TM-TPD (90°). During conduction, the charged TM-TPD molecule underwent conformational relaxation, leading to a dihedral angle change from 90° to 50°, and the TM-TPD molecules tended to be more conjugated (see Supporting Information SI.1 for details). The conjugated electrons of the phenylene rings tended to be shared by single bonds between the phenylene rings, thus enhancing the Raman activity of the molecule (ON mode).

In addition to the voltage and charge states, the Raman signature of TM-TPD was controlled by the illumination geometry. This result confirms previous observations with the OPE-3 molecule[31], demonstrating the versatility of the molecule choice. To explain the switching behaviour and investigate the underlying mechanisms, it was necessary to investigate the near-field angular momentum around the probe tip and its impact on the molecular conformation and Raman response.

Analysis of electromagnetic near field

To fully characterise the electromagnetic near field and the related angular momentum around the probe tip, numerical simulations were performed using the finite-difference time domain (FDTD) method[34]. Both the substrate and the tip shell were gold, while the tip core was silica. Unless otherwise stated, the tip had a TP shape with mirror symmetry along the *x*-axis (Fig. 1). There was a 2-nm gap between the tip and the substrate, and the coordinate origin was located at the gap centre. The incoming illumination was modelled using a Gaussian beam, incident either along the *z*-axis for top illumination or in the *x*–*z*-plane at 45° with respect to the *z*-axis for side illumination. The Gaussian beam was *s*-(*p*-)polarised with an electric (*E*) field parallel (perpendicular) to the *y*-axis.

The effect of the nanostructure is important in the near field. Using *p*-polarised incident light from the left side, the electric field intensity ($|E|^2$) was computed first, as shown in Fig. 3. The main contributor to the intensity was the E_z

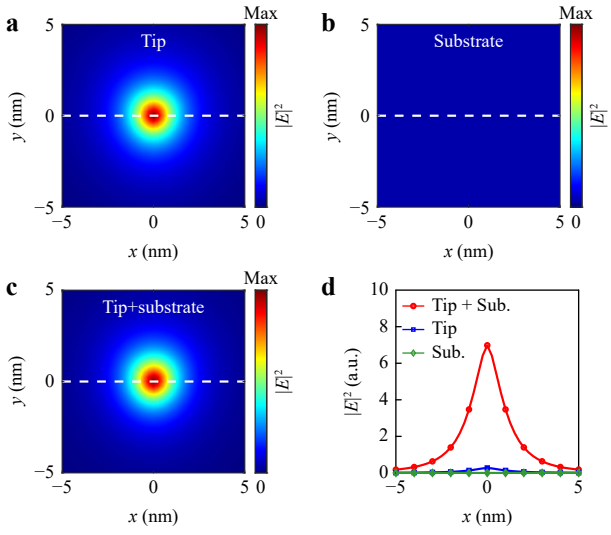

Fig. 3 Electric field intensity distributions of near-field mode for side illumination with different nanostructures. The electric field intensity distributions are shown in the $z = 0$ plane for **a** tip only, **b** substrate only, and **c** tip with substrate. **d** Profile of the electric field intensity at $y = 0$ (white dash lines in **a**–**c**).

component (see Supporting Information SI.2 for details). The combination of both the tip and the substrate is essential to create a cavity and then confine the light tightly when the local surface plasmon is excited, resulting in an enhancement of the near field (Fig. 3c, d).

Such a numerical analysis also makes it possible to discriminate the contributions from the *s*- and *p*-polarised components of the unpolarised laser beam used in the experiments. Fig. 4 shows the electric-field intensity for *s*- and *p*-polarised illumination from both channels (side and top). The gap mode can be excited mainly by *p*-polarisation for side illumination (Fig. 4a–c). Side *s*-polarised illumination leads to a negligible intensity (Fig. 4b) because the gap mode mainly relies on the E_z component. Therefore, this side *s*-pol illumination, without the E_z component, hardly excites the gap mode. Next, top illumination was studied (see Supporting Information SI.3 for further details). The *s*-polarisation was the main contributor to the top illumination (Fig. 4d–f). The top *p*-polarised illumination showed poor excitation of the gap mode owing to the mirror antisymmetry of the electric field along the *x*-axis. Therefore, regarding polarisation, only the contributions of the side *p*-polarised and top *s*-polarised illumination must be further analysed.

After the electromagnetic near field and the polarisation dependency were identified, the impact of the gap mode on the near-field angular momentum was examined. Fig. 5 shows the simulation results of the gap-mode angular momentum excitations for different illuminations and tip structures. The illumination was either side *p*-polarised or top *s*-polarised. In addition to the TP tip, a rectangular pyramid (RP) tip was introduced to illustrate the influence of symmetry on the system. The angular momentum excitation of the gap mode is characterised by the angular momentum density (AMD) distribution, which can be directly obtained as

$$\vec{l} = \vec{r} \times \vec{p} = \varepsilon\mu\left(\vec{r} \times \vec{S}\right) \tag{1}$$

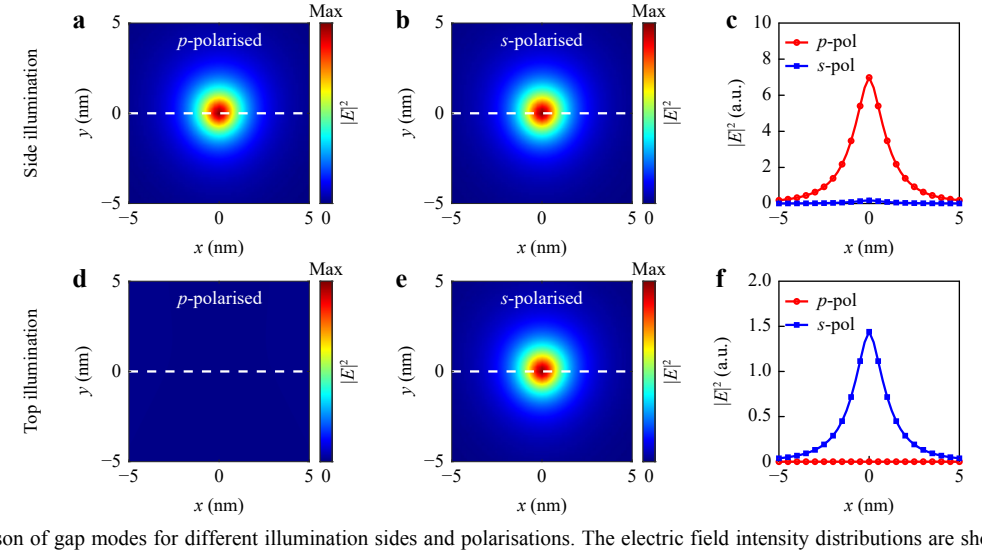

Fig. 4 Comparison of gap modes for different illumination sides and polarisations. The electric field intensity distributions are shown in the $z = 0$ plane for **a** side *p*-pol, **b** side *s*-pol, **d** top *p*-pol, and **e** top *s*-pol illuminations. **c**, **f** Profiles of the electric field intensity at $y = 0$ (white dash lines in **a**, **b**, **d**, **e**).

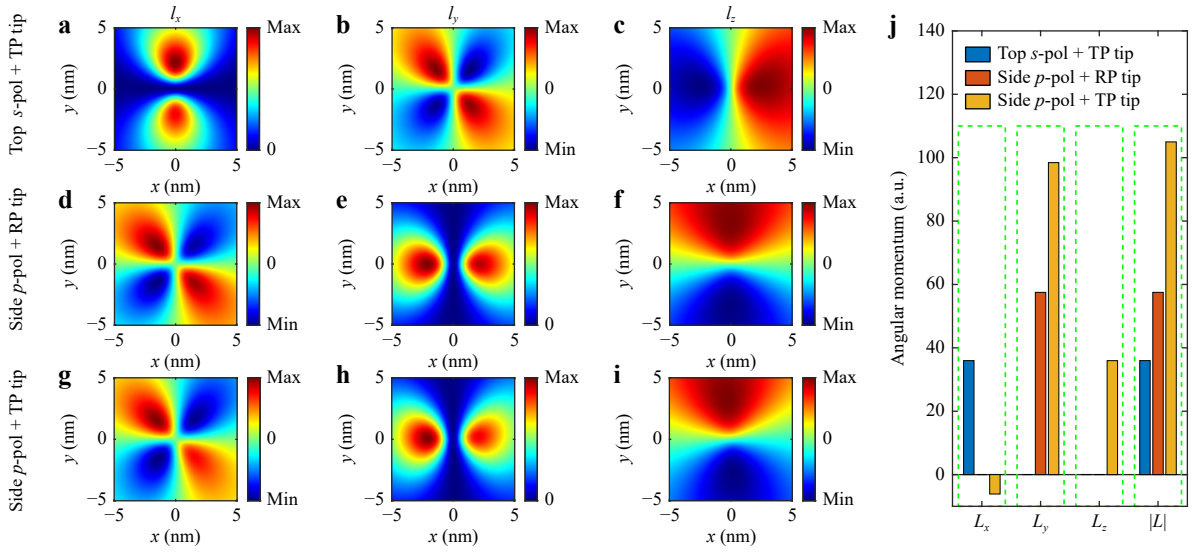

Fig. 5 Comparison of gap-mode angular momentum excitations for different illuminations and tip structures. The components l_i (subscript i is for x, y, z) of the angular momentum density distribution are shown in the $z = 0$ plane for **a**–**c** top s-pol illumination with a TP tip, **d**–**f** side p-pol illumination with a RP tip, and **g**–**i** side p-pol illumination with a TP tip. **j** Total angular momentum $|L|$ and its components L_i. The different illuminations and tip structures result in different angular momentum responses limited by the symmetries of the angular momentum density distribution. Only side p-pol illumination with a TP tip can generate a z-component of angular momentum.

where the vectors of $\vec{r}$, $\vec{p}$, and $\vec{S} = 1/2Re\left(\vec{E} \times \vec{H}^*\right)$ correspond to the position, momentum density, and Poynting vector, respectively, while ε and μ are the electric permittivity and magnetic permeability, respectively. In the case of top s-pol illumination with a TP tip, $\vec{E}$ and the tip structure are symmetric along the x-axis, but $\vec{H}$ is antisymmetric. Therefore, the components of the AMD satisfy the following conditions (see Supporting Information SI.4 for details).

$$\begin{bmatrix} l_x(x) \\ l_y(x) \\ l_z(x) \end{bmatrix} = \begin{bmatrix} l_x(-x) \\ -l_y(-x) \\ -l_z(-x) \end{bmatrix} \tag{2}$$

This indicates that the AMD is antisymmetric along the x-axis in the system, as confirmed numerically in Fig. 5a–c. For side p-pol illumination, an RP tip symmetric along the x- and y-axes can result in better symmetry in the near-field system. Similarly, one can deduce the components of the AMD for side p-pol illumination with an RP tip, which can be expressed as

$$\begin{bmatrix} l_x(y) \\ l_y(y) \\ l_z(y) \end{bmatrix} = \begin{bmatrix} -l_x(-y) \\ l_y(-y) \\ -l_z(-y) \end{bmatrix} \tag{3}$$

Correspondingly, the AMD is antisymmetric along the y-axis, as confirmed by the results shown in Fig. 5d–f. The case for side p-pol illumination with a TP tip has results (Fig. 5g–i) similar to those with the RP tip; however, its AMD distribution is asymmetric along the y-axis, induced by the asymmetry of the TP tip along the y-axis. The near-field angular momentum can be deduced from the AMD as

$$\vec{L} = \int \vec{l} dV \tag{4}$$

(Fig. 5j), where V is the volume of the near-field space. Because of the antisymmetry of the AMD for top s-pol illumination with a TP tip, the y- and z-components of the angular momentum are equal to zero. Side p-pol illumination with an RP tip yields similar results for the x- and z-components. Therefore, these two cases cannot generate angular momentum in the z-direction, which is critical for coupling with the molecule. However, the TP tip breaks the structural symmetry along the y-axis. Accordingly, it results in an asymmetric AMD distribution for side illumination that generates near-field angular momentum in the z-direction (i.e., L_z is nonzero for side p-pol illumination with a TP tip in Fig. 5j).

According to the above analysis, the angular momentum excitation of the gap mode is closely related to the symmetry of the optical system, and some components of the near-field angular momentum can be cancelled by symmetry. Consequently, symmetry must be considered when designing optical systems for applications based on the manipulation of near-field angular momentum.

Impact of near-field angular momentum on molecular conformation and Raman response

As mentioned previously, the Raman activity of TM-

TPD is dominated mainly by the molecular conformation characterised by the dihedral angle between the benzene rings at both ends, and the central benzene ring (angle shown in Fig. 2b and Supporting Information SI.1). In Fig. 6a, the Raman spectra are presented for different dihedral angles from 50° to 90° for a TM-TPD molecule, clearly indicating a decrease in intensity when the angle is larger than 50°, with a minimum of 90°. These results correlate with the relationship between the dihedral angle and the Raman spectrum.

We attribute the observed change in the Raman activity with side illumination when a bias voltage is applied to a similar modification of the dihedral angle of the molecule in the junction. The angular momentum of light causes a torque on the molecule, modifies its conformation, and suppresses the Raman mode (Fig. 2a). More precisely, the change in conformation and the intense Raman signal observed when a bias voltage is applied is reversed when the molecular junction is illuminated from its side.

Specifically, the z-component of the angular momentum can produce a torque $\vec{\tau} = d\vec{L}/dt$ along the z-direction. For top illumination, the z-component of the angular momentum is zero (Fig. 5j); thus, the molecular conformation is unaffected, and the Raman activity is influenced by the biased voltage only. However, Raman activity is significantly different under side illumination. Because of the nonzero L_z component for side illumination (Fig. 5j), torque is produced in the z-direction. This torque causes the molecule to follow a rotational motion, breaking down the electron density rearrangement caused by the biased voltage and rendering the conjugation vibration Raman inactive again. This change in the conformation of the molecule under side illumination is possible because of the low energy barrier of rotation of the charged molecule (see Figure S1 in the Supporting Information). Consequently, the Raman intensity of the molecular junction falls below the detection limit. It is, therefore, expected that the Raman signature of TM-TPD can be increased by temporal charging and then depressed if coupled with the angular momentum of the light where the π-conjugated character is dominant.

To confirm the mechanism behind the switching behaviour of the molecular junction induced by the near-field angular momentum transfer to the molecule, combined side/top illumination characterisation was performed. From the simulation presented above, asymmetry in the electromagnetic field is reintroduced in such an illumination geometry, causing a nonzero angular momentum in the z-direction and producing a z-axis torque acting on the molecule. Accordingly, it was found experimentally that the Raman peak disappeared again when side illumination was added to the well-established molecular junctions monitored with top-illumination Raman spectroscopy (bottom curve, Fig. 6b). Side illumination was introduced with only 1% of the energy of the top illumination, and the Raman spectra were

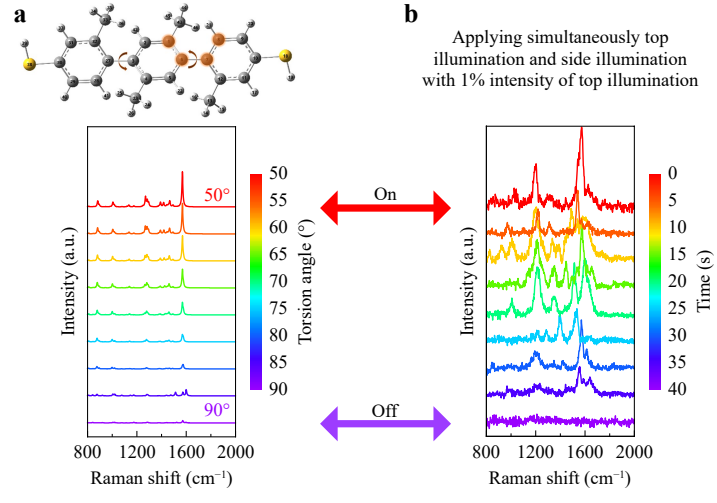

Fig. 6 Raman investigation of the molecular junction with both top and side illumination. **a** Raman spectra for TM-TPD molecule calculated at the B3LYP-D3(BJ)/6-31G(d,p) level with different dihedral angles. The four carbon atoms associated with the dihedral angle are marked in brown. The Raman spectra change simultaneously with the variation in the dihedral angle from 50° (ON mode) and almost disappear at 90° (OFF mode). **b** Change of Raman spectra of the 1.0-V biased molecular junction continuous under top illumination and side illumination with 1% intensity of top illumination. The Raman peak positions shift progressively, and the intensities of the Raman spectra decrease to be finally turned from ON mode to OFF mode completely after 40 s.

monitored over time. The Raman spectrum of the current-driven molecular junction was initially monitored using only top-illumination geometry (ON mode at t = 0 s). When the side illumination channel was added, the Raman peak position shifted progressively, and the intensity of the Raman spectra decreased, finally turning off completely (OFF mode) after 40 s. The top illumination can turn the Raman mode ON because of the symmetry of the near-field system; however, the symmetry is broken when 1% intensity from side illumination is added to the system, and the conformation of the TM-TPD molecule is gradually changed to depress the Raman mode. For the turning-OFF process, the molecular junction exhibits a dynamic vibrational process. However, the theoretical DFT calculations were performed based on the static state of the stable conformations. The measured signals were not very strong and were easily affected by noise; thus, the experimental results did not perfectly match the calculated results. The turning-OFF process shows that the molecular junction is coupled progressively with the angular momentum of light and progressively changes the dihedral angle and, consequently, the Raman intensity. Furthermore, the Raman modes can be turned ON again in the single-molecule junction after switching OFF. The reproducibility of the process was confirmed experimentally.

Conclusion

It was shown that conformational molecular junctions can be controlled not only by the voltage applied to a single-molecule junction but also by the optical angular momentum in the near field, which is enhanced by the plasmon gap mode in the junction. A bias voltage exceeding 1.0 V results in an electron density rearrangement of the molecular junction, which activates the Raman mode. This Raman mode is enhanced by planarisation and increased π-conjugation of the TM-TPD molecule. In striking contrast to top illumination, side illumination of the junction leads to the absence of a detectable Raman signal for all biased voltages. The angular momentum of light causes a z-axis torque when the distribution of the electromagnetic field is asymmetric. This makes it possible to change the conformation of the TM-TPD, destroys the transport electron density rearrangement, and finally suppresses the Raman mode. These studies made it possible to identify experimentally that the optical angular momentum is a driving force for molecular switching. This conclusion was reached based on detailed numerical simulations of the near-field EM field. More precisely, it was found that the angular momentum excitation has a very close link with the symmetry of the near-field system. This study opens up new avenues for research on molecular logic and optical angular momentum in the near-field regime. The possibility of addressing physicochemical phenomena with a single-molecule resolution shown in this study serves as a departure point for a new generation of nanomechanical studies using MJS setups. Technologically, these investigations demonstrated single-molecule monitoring and manipulation with excellent control, opening new avenues for multilogic single-molecule computing.

Acknowledgements

The research described in this article was supported by the National Key Research and Development Program of China (No. 2021YFE0115700), Guangdong Basic and Applied Basic Research Foundation (Nos. 2020A1515110709, 2020A1515110712, and 2020B1515120068), and Jihua Youth Innovation Fund (No. X201021XF200). The authors acknowledge support from the WBI – MOST agreement. M.L. is a Research Associate of the Fonds de la Recherche Scientifique – FNRS.

Author details

[1]Jihua Laboratory, No.28 Huandao South road, Nanhai district, Foshan 528200, China. [2]Department of Physics and Namur Institute of Structured Materials, University of Namur, Rue de Bruxelles 61, 5000 Namur, Belgium. [3]MIIT Key Laboratory of Critical Material Technology for New Energy Conversion and Storage, School of Chemistry and Chemical Engineering, Harbin Institute of Technology, Harbin 150001, China

Author contributions

JZ carried out the analytical modelling, FDTD simulations, result analysis, and article writing. ML, LH, CW, and XW studied the theoretical and numerical aspects and interpreted the results. ZL carried out the DFT calculations, sample fabrication, and measurements. As the principal investigator of the projects, HB conceived the idea, suggested the designs, and planned, coordinated, and supervised the work.

Conflict of interest

Hai Bi is an Editor for the journal, and no other author has reported any competing interests.

Supplementary information is available for this paper at https://doi.org/10.37188/lam.2023.034.

Received: 12 December 2022 Revised: 22 September 2023 Accepted: 26 September 2023

Accepted article preview online: 27 September 2023

Published online: 29 September 2023

References

1. Wu, S. M. et al. Molecular junctions based on aromatic coupling. *Nature Nanotechnology* **3**, 569-574 (2008).
2. Aradhya, S. V. & Venkataraman, L. Single-molecule junctions beyond electronic transport. *Nature Nanotechnology* **8**, 399-410 (2013).
3. Frisenda, R. & van der Zant, H. S. J. Transition from strong to weak electronic coupling in a single-molecule junction. *Physical Review Letters* **117**, 126804 (2016).
4. Nitzan, A. & Ratner, M. A. Electron transport in molecular wire junctions. *Science* **300**, 1384-1389 (2003).
5. Betzig, E. & Trautman, J. K. Near-field optics: microscopy, spectroscopy,

and surface modification beyond the diffraction limit. *Science* **257**, 189-195 (1992).
6. Nie, S. M. & Emory, S. R. Probing single molecules and single nanoparticles by surface-enhanced Raman scattering. *Science* **275**, 1102-1106 (1997).
7. Pettinger, B. et al. Nanoscale probing of adsorbed species by tip-enhanced Raman spectroscopy. *Physical Review Letters* **92**, 096101 (2004).
8. Saikin, S. K. et al. On the chemical bonding effects in the Raman response: benzenethiol adsorbed on silver clusters. *Physical Chemistry Chemical Physics* **11**, 9401-9411 (2009).
9. Fischer, U. C. & Pohl, D. W. Observation of single-particle plasmons by near-field optical microscopy. *Physical Review Letters* **62**, 458-461 (1989).
10. Claridge, S. A., Schwartz, J. J. & Weiss, P. S. Electrons, photons, and force: quantitative single-molecule measurements from physics to biology. *ACS Nano* **5**, 693-729 (2011).
11. Cocker, T. L. et al. Tracking the ultrafast motion of a single molecule by femtosecond orbital imaging. *Nature* **539**, 263-267 (2016).
12. Nguyen, H. A. et al. STM imaging of localized surface plasmons on individual gold nanoislands. *The Journal of Physical Chemistry Letters* **9**, 1970-1976 (2018).
13. Wallum, A., Nguyen, H. A. & Gruebele, M. Excited-state imaging of single particles on the subnanometer scale. *Annual Review of Physical Chemistry* **71**, 415-433 (2020).
14. Zhang, R. et al. Chemical mapping of a single molecule by Plasmon-enhanced Raman scattering. *Nature* **498**, 82-86 (2013).
15. Yampolsky, S. et al. Seeing a single molecule vibrate through time-resolved coherent anti-Stokes Raman scattering. *Nature Photonics* **8**, 650-656 (2014).
16. Gerster, D. et al. Photocurrent of a single photosynthetic protein. *Nature Nanotechnology* **7**, 673-676 (2012).
17. Bi, H. et al. Voltage-driven conformational switching with distinct Raman signature in a single-molecule junction. *Journal of the American Chemical Society* **140**, 4835-4840 (2018).
18. Kharintsev, S. S. et al. Experimental evidence for axial anisotropy beyond the diffraction limit induced with a bias voltage plasmonic nanoantenna and longitudinal optical near-fields in photoreactive polymer thin films. *ACS Photonics* **1**, 1025-1032 (2014).
19. Saikin, S. K. et al. Separation of electromagnetic and chemical contributions to surface-enhanced Raman spectra on nanoengineered plasmonic substrates. *The Journal of Physical Chemistry Letters* **1**, 2740-2746 (2010).
20. Kharintsev, S. S. et al. Near-field Raman dichroism of azo-polymers exposed to nanoscale dc electrical and optical poling. *Nanoscale* **8**, 19867-19875 (2016).
21. Pozzi, E. A. et al. Ultrahigh-vacuum tip-enhanced Raman spectroscopy. *Chemical Reviews* **117**, 4961-4982 (2017).
22. Pozzi, E. A. et al. Tip-enhanced Raman imaging: an emergent tool for probing biology at the nanoscale. *ACS Nano* **7**, 885-888 (2013).
23. Zhao, Z. K. et al. Shaping the atomic-scale geometries of electrodes to control optical and electrical performance of molecular devices. *Small* **14**, 1703815 (2018).
24. Wang, M. N. et al. Plasmonic phenomena in molecular junctions: principles and applications. *Nature Reviews Chemistry* **6**, 681-704 (2022).
25. Gersten, J. & Nitzan, A. Electromagnetic theory of enhanced Raman scattering by molecules adsorbed on rough surfaces. *Journal of Chemical Physics* **73**, 3023-3037 (1980).
26. Bliokh, K. Y., Smirnova, D. & Nori, F. Quantum spin Hall effect of light. *Science* **348**, 1448-1451 (2015).
27. Rodríguez-Fortuño, F. J. et al. Lateral forces on circularly polarizable particles near a surface. *Nature Communications* **6**, 8799 (2015).
28. Alexandrescu, A., Cojoc, D. & Di Fabrizio, E. Mechanism of angular momentum exchange between molecules and Laguerre-Gaussian beams. *Physical Review Letters* **96**, 243001 (2006).
29. Wu, T., Wang, R. Y. & Zhang, X. D. Plasmon-induced strong interaction between chiral molecules and orbital angular momentum of light. *Scientific Reports* **5**, 18003 (2015).
30. Govorov, A. O., Zhang, H. & Gun'ko, Y. K. Theory of photoinjection of hot plasmonic carriers from metal nanostructures into semiconductors and surface molecules. *The Journal of Physical Chemistry C* **117**, 16616-16631 (2013).
31. Bi, H. et al. Optically induced molecular logic operations. *ACS Nano* **14**, 15248-15255 (2020).
32. Bi, H. et al. Electron–phonon coupling in current-driven single-molecule junctions. *Journal of the American Chemical Society* **142**, 3384-3391 (2020).
33. Bi, H. et al. Single molecules in strong optical fields: a variable-temperature molecular junction spectroscopy setup. *Analytical Chemistry* **93**, 9853-9859 (2021).
34. Yee, K. Numerical solution of initial boundary value problems involving maxwell's equations in isotropic media. *IEEE Transactions on Antennas and Propagation* **14**, 302-307 (1966).